Nematode germ granule assembly is linked to mRNA repression

Scott Takeo Aoki[1], Sarah L Crittenden[1,2], Tina R Lynch[1], Craig A Bingman[1], Marvin Wickens[1], Judith Kimble[1,2,*]

[1] Department of Biochemistry and [2] Howard Hughes Medical Institute, University of Wisconsin-Madison, Madison, WI, USA

* For correspondence:
Judith Kimble
HHMI/Department of Biochemistry
University of Wisconsin-Madison
433 Babcock Drive
Madison, WI 53706-1544
Tel 608-262-6188
Fax 608-265-5820
jekimble@wisc.edu

Keywords: RNA-protein granule, germ granule, scaffold protein

Abbreviations: RNA, ribonucleic acid; UTR, untranslated region; GFP, green fluorescent protein; CRISPR, Clustered Regularly Interspaced Short Palindromic Repeats

Summary

RNA-protein (RNP) granules are non-membrane bound organelles with enigmatic roles in RNA metabolism. Metazoa contain RNP “germ granules” specialized for germline development. *Caenorhabditis elegans* P-granules are liquid droplet germ granules that require PGL proteins for assembly. Here we investigate PGL proteins to understand the relationship between P-granule assembly and germline function. We determine the crystal structure of a PGL N-terminal domain (NTD) and find that it dimerizes. From the structure, we identify mutations that disrupt PGL dimerization *in vitro* and prevent PGL granule formation in mammalian cells in culture. These same mutations in nematodes prevent assembly of PGL into P-granules and cause sterility. Using a protein-mRNA tethering assay, we show that mRNAs recruited to PGL-1 are repressed, while mRNAs recruited to PGL-1 mutants defective for granule assembly are expressed. Therefore, the effects of PGL on mRNA repression and fertility are tightly linked to its formation of higher-ordered assemblies.

Introduction

Subcellular localization can be critical for RNA control. The locations of RNAs and RNA regulatory proteins within a cell can dictate whether RNAs are translated or repressed (Singh et al., 2015). RNA-protein (RNP) granules are non-membrane bound "organelles" found ubiquitously in cells. These granules can be relatively inert, with little exchange of components between the granules and their environment, or they can behave as liquid droplets, with components capable of freely diffusing between the granule and cytoplasm (Hyman et al., 2014; Wu and Fuxreiter, 2016). RNP granules contain factors that regulate mRNA turnover, sequestration and translation and have been proposed to function in mRNA regulation (Buchan, 2014). Yet despite intense interest, the connection between granule assembly and biological function is poorly understood.

Metazoan germ cells contain specialized RNP germ granules with functions in RNA metabolism and small regulatory RNA biogenesis (Voronina et al., 2011). *Caenorhabditis elegans* germ granules, called P-granules, are necessary for adult germ cell maintenance and totipotency (Strome and Updike, 2015). P-granules display liquid droplet behavior (Brangwynne et al., 2009) and have similarities in subcellular location and composition to germ granules in *Drosophila* and vertebrates (Voronina et al., 2011). In adult germ cells (**Figure 1A**), P-granules localize to the cytoplasmic face of nuclear pores and contain mRNAs and proteins involved in RNA metabolism (Updike and Strome, 2010). Yet the molecular function of P-granules is poorly defined. One suggested role has been mRNA repression. This idea is based on localization of repressed mRNAs to P-granules (Schisa et al., 2001) and upregulation of aberrant transcript expression when P-granules are lost (Campbell and Updike, 2015; Knutson et al., 2017; Updike et al., 2014). Because these lines of evidence are indirect and based on gene knockouts of major P-granule assembly proteins, it remains unclear whether transcript repression depends on P-granule components or their assembly into granules.

P-granule formation relies on key assembly proteins. Crucially important are the PGL-1 and PGL-3 proteins (Kawasaki et al., 2004; Kawasaki et al., 1998), close paralogs we henceforth refer to as PGL. PGL protein contains a central dimerization domain (DD) and C-terminal low complexity RGG repeats (**Figure 1B**) (Aoki et al., 2016; Kawasaki et al., 2004; Kawasaki et al., 1998). Genetic removal of PGL causes mislocalization of P-granule proteins (Amiri et al., 2001), aberrant expression of spermatogenic and somatic mRNAs (Campbell and Updike, 2015; Knutson et al., 2017; Updike et al., 2014), and temperature-dependent sterility (Kawasaki et al., 2004; Kawasaki et al., 1998). PGL proteins self assemble into granules, both *in vitro* using purified recombinant protein (Saha et al., 2016), and in intestinal nematode cells or mammalian cells in culture when expressed on their own (Hanazawa et al., 2011; Updike et al., 2011). These artificial PGL granules display liquid droplet behavior (Saha et al., 2016), indicating that

PGL protein alone is sufficient to recapitulate the biophysical properties of P-granules in nematode cells (Brangwynne et al., 2009). Many RNP granule assembly proteins rely on low complexity sequences for low affinity, multivalent interactions (Banani et al., 2017). PGL lacks large regions of low complexity, with the exception of its C-terminal RGG repeats that are not necessary for granule formation (Hanazawa et al., 2011; Saha et al., 2016). The central DD domain can dimerize (Aoki et al., 2016), but higher ordered assembly demands additional protein contacts.

P-granules serve as a paradigm for RNP granules with liquid droplet properties. We have investigated the PGL assembly protein to understand PGL multimerization into a granule and to probe the relationship between granule formation and its biological function. We determined the structure of the PGL N-terminal domain (NTD), found that it dimerizes and identified amino acids required for NTD dimerization that are also required for PGL assembly into granules *in vitro*, in mammalian culture cells and germ cells in living nematodes. Indeed, PGL multimerization is critical for nematode fertility. Using a protein-mRNA tethering assay in living nematodes, we show that reporter mRNAs recruited to PGL are repressed, and that their repression requires PGL assembly into granules. This study therefore provides direct *in vivo* evidence that RNP granule formation is linked to mRNA repression.

Results

Structure determination of a second PGL dimerization domain

Granule formation is driven by multimer-multimer interactions (Bergeron-Sandoval et al., 2016). The central PGL DD provides one multimerization site (Aoki et al., 2016), but since PGL protein alone can form granules (Hanazawa et al., 2011; Saha et al., 2016), we postulated the existence of another PGL multimerization region critical for granule assembly. The region N-terminal to DD (**Figure 1B**) had high sequence conservation (**Figure S1A**), implying a critical

role in PGL function. Our initial efforts to express trypsin-mapped recombinant protein fragments of this N-terminal region proved unfruitful. However, we had noticed that the original DD N-termini were disordered in crystal structures (Aoki et al., 2016). When the N-terminal recombinant protein was extended to include these disordered residues (**Figure S1A**), we obtained robust expression sufficient for biochemical and structural characterization (**Figure S2A-B**). Henceforth, we refer to this stable protein fragment as the N-terminal domain (NTD) (**Figure 1B**).

We determined the *C. japonica* PGL-1 NTD crystal structure to 1.5 Å (**Figure 1C-D**, see **Table S1** for statistics, see Methods for further details on crystallization and structure determination). The NTD had a novel fold consisting of 11 alpha helices and a single N-terminal beta strand (**Figure 1D**). The crystal asymmetric unit (ASU) was composed of four NTD domains (**Figure 1C**). These four NTDs were structurally similar (RMSD 0.219 - 0.254, chains B-D aligned to A), except for minor differences in their termini and internal loops. More relevant, they possessed two pairs of identical interfaces (**Figure 1C**). One of these interface pairs consisted of a network of conserved amino acid side chains making extensive salt bridges and hydrogen bonds (**Figures 2A-C and S2C-E**). The complexity and conservation of these interactions suggested biological relevance. We first tested for dimerization *in vitro*. Recombinant PGL-3 NTD formed a dimer on a sizing column combined with multi-angle light scattering (SEC-MALS, **Figure 2D-E**). We postulated that the conserved interface in the NTD crystal structure might be its dimerization interface. To test that idea, we used our structural model and *in silico* prediction (Kortemme et al., 2004) to design missense mutations that disrupt the interface. These analyses yielded two distinct mutants: K126E K129E with two mutated residues and R123E with a single mutated residue. Both NTD mutants formed monomers rather than dimers in solution (**Figure 2D-E**). We conclude that the dimers observed in the crystal structure represent the NTD dimer detected in solution.

PGL NTD dimerization is critical for granule formation

To assess the role of NTD dimerization in PGL granule self-assembly, we first turned to an assay in mammalian cells where PGL expressed alone assembles into granules (Hanazawa et al., 2011). Similar to that report, GFP-tagged PGL-1 formed large cytoplasmic granules in cells (**Figure 2F-G**), while GFP alone was diffuse (**Figure 2H**). However, if we mutated the GFP-tagged PGL-1 to either K126E K129E or R123E, PGL-1 no longer formed granules (**Figure 2I-J**). We conclude that NTD dimerization is essential for self-assembly of PGL granules in mammalian cells.

We next asked whether NTD dimerization was essential for PGL function and granule assembly in the nematode germline. We inserted a SNAP tag (Keppler et al., 2003) using CRISPR gene editing (Paix et al., 2015) at the endogenous *pgl-1* locus (**Figure 3A and S1B**). Wild-type PGL-1 (N2) and PGL-1::SNAP were similarly fertile at 20°C and 25°C (**Figure 3B**); in contrast, a *pgl-1* null mutant was mostly sterile at 25°C (**Figure 3B**), as reported previously (Kawasaki et al., 2004; Kawasaki et al., 1998). SNAP-tagged PGL-1 permitted visualization of the protein with essentially no background (**Figure 3C-D**). PGL-1::SNAP assembled into cytoplasmic granules at the nuclear periphery (**Figure 3D**), similar to those seen with antibody staining to untagged PGL-1 and PGL-3 (Kawasaki et al., 2004; Kawasaki et al., 1998). The SNAP-tagged protein therefore provides a simple way to evaluate PGL assembly into granules.

To probe the role of PGL NTD dimerization in the nematode germline, we introduced the assembly mutants into PGL-1::SNAP (**Figure S1B**) and assayed effects on fertility and granule formation. For both K126E K129E and R123E mutants, many were sterile at 20°C and nearly all were sterile at 25°C (**Figure 3B**). Indeed, the percentage of sterile animals was higher than seen in a *pgl-1* null mutant (**Figure 3B**), suggesting that abolishing NTD dimerization had a

dominant-negative effect. Both interface mutants had smaller than normal germlines and many lacked oocytes (**Figure S3B-D**), similar to *pgl-1* and *pgl-1 pgl-3* null mutant germlines (Kawasaki et al., 2004; Kawasaki et al., 1998). We next examined expression and localization of mutant SNAP-tagged PGL-1 proteins, in both fertile (**Figure 3**) and sterile germlines (**Figure S3**). Both K126E K129E and R123E mutant proteins were expressed, but their distribution was largely diffuse (**Figures 3E-F and S3F-G**). The mutant proteins did form small perinuclear granules in some germ cells of all gonads imaged (**Figure 3E-F and S3F-G**), and for each mutant we found a single germline (1/59 for K126E K129E; 1/54 for R123E) with small PGL-1 perinuclear granules in all germ cells (**Figure S3H-I**). Therefore, both PGL-1 mutant proteins are capable of incorporating into P-granules, but do so much more weakly than their wild-type counterparts (**Figure 3D**). We conclude that PGL NTD dimerization is critical for fertility and efficient PGL granule formation.

We wondered why sterility of PGL-1 NTD dimerization mutants was more severe than that of a *pgl-1* null mutant. One plausible explanation was interference with assembly of other P-granule components into granules, which might yield dominant-negative effects. Normally, PGL-1 interacts with PGL-3 (Kawasaki et al., 2004), and both PGL-1 and PGL-3 rely on GLH-1 or GLH-4 Vasa helicases to localize to the nuclear periphery (Spike et al., 2008; Updike et al., 2011). In contrast, GLH proteins assemble at the nuclear pore independently of PGLs (Kawasaki et al., 2004; Kawasaki et al., 1998; Kuznicki et al., 2000). We postulated that PGL-1 assembly mutants might interfere with assembly of PGL-3 into granules but not affect GLH-1 localization. To test this idea, we epitope-tagged endogenous *pgl-3* and *glh-1* (see Methods) and compared localization of PGL-3::V5 and GLH-1::Myc in germ cells expressing wild type PGL-1::SNAP or mutant PGL-1::SNAP K126E K129E. With wild-type PGL-1::SNAP, all three proteins, PGL-1, PGL-3 and GLH-1, co-localized in granules at the nuclear periphery (**Figure 3G-K**), as previously observed for untagged proteins (Kawasaki et al., 2004; Kuznicki et al., 2000).

However, with mutant PGL-1::SNAP, the wild-type PGL-3 protein became diffuse with occasional small perinuclear granules, a distribution similar to PGL-1 mutant protein (**Figure 3L-N**). By contrast, GLH-1 localized at the nuclear periphery independent of PGL-1 or PGL-3 (**Figure 3O-P**). Therefore, the PGL-1 assembly mutant affected PGL-3 assembly and incorporation into P-granules, but it did not abolish GLH-1 localization. Because the percent sterility of PGL-1 K126E K129E mutants was similar to that of *pgl-1 pgl-3* double null mutants (Kawasaki et al., 2004), we suggest that the severe sterility of PGL-1 NTD mutants results from effects on both PGL-1 and PGL-3 assembly into granules.

Granular PGL represses mRNAs *in vivo*

Prior studies have suggested that P-granules regulate mRNA expression (see Introduction). To directly test whether P-granules can regulate mRNAs, we relied on a protein-mRNA tethering assay, widely used to investigate RNA regulatory proteins (Baron-Benhamou et al., 2004; Coller and Wickens, 2002). Our assay examined the fate of mRNAs to which PGL-1 was tethered via λN22, a short peptide that binds with high affinity and sequence specificity to the boxB RNA hairpin (Baron-Benhamou et al., 2004). Versions of this method were used previously in worms and other organisms (Baron-Benhamou et al., 2004; Wedeles et al., 2013). For the reporter, we inserted three boxB sites into the 3'UTR of a ubiquitously-expressed, germline GFP-histone reporter (**Figure 4A**, Methods) (Zeiser et al., 2011). To tether PGL to the GFP reporter mRNA, we inserted the λN22 peptide sequence into our PGL-1::SNAP protein (**Figures 4A** and **S1B,** Methods). Addition of λN22 to PGL-1 rendered homozygous worms sterile (0% fertile, n=94), but the λN22-tagged *pgl-1* gene could be maintained and tested as a fertile heterozygote (PGL-1::SNAP::λN22/+). The logic of our strategy is simple: if tethered wild-type PGL-1 represses GFP expression, we can then test assembly-defective PGL-1 to ask if repression relies on granule formation (**Figure 4A**).

We assayed reporter expression in both living animals and fixed, extruded gonads. In living animals harboring both reporter and PGL-1::SNAP without λN22, GFP was expressed robustly (**Figures 4B**), but in those with both reporter and PGL-1::SNAP::λN22, GFP was absent (**Figure 4C**). When fixed, control germlines expressed GFP robustly (**Figure 4E**), but those with PGL-SNAP::λN22 had either no detectable GFP (**Figure 4F**) or extremely faint GFP (2/39 germline). The wild-type PGL-1::SNAP::λN22 formed perinuclear granules (**Figure 4E-F**), though the SNAP signal was lower, perhaps because animals were heterozygous. Regardless, the key conclusion is that PGL-1 tethering dramatically decreased GFP expression from the mRNA reporter.

One possible explanation for loss of GFP expression might have been germline silencing, a phenomenon common for genes expressing foreign proteins and thought to prevent deleterious mRNAs from entering the cytoplasm (Hoogstrate et al., 2014). To ask if the reporter had been silenced, we used single molecule fluorescence *in situ* hybridization (smFISH) to detect *gfp* RNAs. Control germ cells harboring PGL-1::SNAP without λN22 (**Figure S4A-D**) possessed nuclear and cytoplasmic puncta (**Figure S4D**). We interpret the nuclear puncta as active transcription sites and cytoplasmic puncta as mRNAs, based on a previous study (Lee et al., 2016). In these control germ cells, GFP protein fluorescence was robust (**Figure S4B**), and PGL-1::SNAP localized to perinuclear granules (**Figure S4C**). Germ cells harboring PGL-1::SNAP::λN22 (**Figure S4E-H,M**) also possessed nuclear and cytoplasmic puncta (**Figure S4H,M**), but cytoplasmic puncta were fewer and frequently colocalized with P-granules (**Figure S4G-H,M**). These germ cells possessed *gfp* reporter transcripts and thus were not subject to germline silencing. However, they had no GFP protein expression, indicating that reporter expression was repressed by PGL-1 tethering.

Our structural insight into PGL provided an opportunity to test how PGL granule formation affected its ability to repress mRNAs. We introduced K126E K129E into PGL-1::SNAP::λN22 to prevent robust granule assembly (**Figure S1B**). Mutant homozygotes had modest fertility (21% fertile, n=96) that was comparable to other NTD mutant worms (**Figure 3B**). Dimerization-defective PGL-1 failed to repress the reporter RNA to which it was tethered: most germ cells expressed GFP, both in living worms (**Figure 4D**) and fixed gonads (**Figure 4G**). The PGL-1 mutant protein was diffuse and non-granular (**Figure 4G**), as expected. By smFISH for gfp reporter RNA, germ cells with mutant PGL-1::SNAP::λN22 had large puncta in their nuclei and small puncta throughout their cytoplasm (**Figure S4I-L**), similar to gonads expressing PGL-1::SNAP without λN22 (**Figure S4A-D**). Formally, the PGL-1 interface residue mutations might affect granule assembly and mRNA repression independently. However, the simplest explanation is that PGL-1 must assemble into granules for mRNA repression.

Discussion

P-granules are paradigmatic liquid droplet RNP granules and have been predicted to be sites of mRNA repression. This idea was based on several observations. Repressed mRNAs appear trapped in P-granules (Schisa et al., 2001); P-granules are necessary to repress aberrant expression of spermatogenic and somatic transcripts (Campbell and Updike, 2015; Knutson et al., 2017; Updike et al., 2014); and P-granule components include inhibitory RNA binding proteins, like the Pumilio homolog, FBF-2 (Voronina et al., 2012) and RNA regulatory enzymes, like the Argonaut/Piwi PRG-1 (Batista et al., 2008) and the deadenylase PARN-1 (Tang et al., 2016). In this work, we report the discovery of PGL NTD dimerization and demonstrate that PGL NTD dimerization is critical for granule formation, fertility and mRNA repression *in vivo*. Based on these results, we propose that mRNAs in P-granules are repressed and that this repression requires PGL assembly into granules (**Figure 4H)**. PGL contains two dimerization domains (this work; Aoki et al., 2016), but mutations disrupting DD dimerization have been elusive. A critical

future direction is to investigate how each dimerization domain contributes to higher order and likely oligomeric assembly.

Granule assembly proteins form a structural network that relies on multivalency and low affinity interactions for plasticity (Bergeron-Sandoval et al., 2016). We have discovered that PGL uses at least one dimerization domain to form granules, but our results do not address the low affinity interactions that must be present to drive liquid droplet behavior. Critical granule assembly proteins have been identified for several RNP granules. Examples include Oskar and Vasa for *Drosophila* polar granules (Breitwieser et al., 1996; Markussen et al., 1995; Vanzo and Ephrussi, 2002), EDC3 and LSM4 for P-bodies (Decker et al., 2007), and MEG-3 and MEG-4 for embryonic P-granules (Wang et al., 2014). These examples rely on a combination of multimerization domains and low complexity, intrinsically disordered sequences to facilitate granule formation (Decker et al., 2007; Jeske et al., 2015; Ling et al., 2008; Nott et al., 2015; Wang et al., 2014). We suggest that PGL also makes low affinity contacts that work with its dimerization interfaces to facilitate granule formation. Recombinant PGL proteins make granules on their own *in vitro* (Saha et al., 2016), suggesting that PGL has low affinity contacts in the full-length protein. RGG repeats facilitate granule formation in other assembly proteins (Nott et al., 2015), but PGL did not require its RGG repeats to form granules in mammalian cell culture (Hanazawa et al., 2011). The RGG repeats may instead be needed to trigger robust granule assembly with RNA (Saha et al., 2016) or impart liquid droplet properties associated with PGL in nematodes (Brangwynne et al., 2009).

Our study provides direct evidence that recruiting mRNAs to a liquid droplet RNP granule represses their expression. The mechanism of repression remains unclear. P-granule components include RNA turnover enzymes and translation inhibitory proteins (Updike and Strome, 2010) that may repress PGL-tethered mRNAs directly. Alternatively, tethered mRNAs

may be trapped within granules by avidity to high PGL concentrations, blocking their access to translational machinery. Regardless, this work adds to the emerging theme that granules play a general role in repression. Liquid droplet stress granules sequester the mTORC1 protein complex to block activation of mTOR signaling (Wippich et al., 2013). Mammalian cells can trap hormones and melanin in amyloid-like aggregates to prevent signaling (Fowler et al., 2006; Maji et al., 2009). RNP granules have also been proposed to repress mRNAs. mRNA repressors are found in RNP granules (e.g. DDX6/Dhh1, Decker and Parker, 2012) but their repressive activities can function independently of granules (Carroll et al., 2011). Granule formation of a yeast amyloid-like RNA binding protein correlates with translational inhibition of transcripts critical for gametogenesis (Berchowitz et al., 2015), and P-bodies contain mRNAs that are translationally repressed in cells (Hubstenberger et al., 2017). Further studies that pair insights into mechanisms of granule assembly with direct *in vivo* assays of regulation will be pivotal moving forward to decipher the mechanistic function of other RNP granules in their natural biological context.

Acknowledgements

The authors thank M. Cox for equipment; J. Claycomb for plasmids and strains; T. Hoang, S. Strome, D. Updike, and members of the Kimble and Wickens labs for helpful discussions. Use of the LS-CAT Sector 21 was supported by the Michigan Economic Development Corporation and the Michigan Technology Tri-Corridor (Grant 085P1000817). The Keck Biophysics Facility (SEC-MALS) is supported in part by NCI CCSG P30 CA060553 grant awarded to the Robert H Lurie Comprehensive Cancer Center. STA was supported by K99HD081208. CAB was supported by NIH grants GM094584, GM094622 and GM098248. MW was supported by NIH grant GM50942. JK is an Investigator of the Howard Hughes Medical Institute.

References

Amiri, A., Keiper, B.D., Kawasaki, I., Fan, Y., Kohara, Y., Rhoads, R.E., and Strome, S. (2001). An isoform of eIF4E is a component of germ granules and is required for spermatogenesis in *C. elegans*. Development *128*, 3899-3912.

Aoki, S.T., Kershner, A.M., Bingman, C.A., Wickens, M., and Kimble, J. (2016). PGL germ granule assembly protein is a base-specific, single-stranded RNase. Proc. Natl. Acad. Sci. USA *113*, 1279-1284.

Banani, S.F., Lee, H.O., Hyman, A.A., and Rosen, M.K. (2017). Biomolecular condensates: organizers of cellular biochemistry. Nat. Rev. Mol. Cell Biol. *18*, 285-298.

Baron-Benhamou, J., Gehring, N.H., Kulozik, A.E., and Hentze, M.W. (2004). Using the λN peptide to tether proteins to RNAs. Methods Mol. Biol. *257*, 135-154.

Batista, P.J., Ruby, J.G., Claycomb, J.M., Chiang, R., Fahlgren, N., Kasschau, K.D., Chaves, D.A., Gu, W., Vasale, J.J., Duan, S.*, et al.* (2008). PRG-1 and 21U-RNAs interact to form the piRNA complex required for fertility in *C. elegans*. Mol. Cell *31*, 67-78.

Berchowitz, L.E., Kabachinski, G., Walker, M.R., Carlile, T.M., Gilbert, W.V., Schwartz, T.U., and Amon, A. (2015). Regulated formation of an amyloid-like translational repressor governs gametogenesis. Cell *163*, 406-418.

Bergeron-Sandoval, L.P., Safaee, N., and Michnick, S.W. (2016). Mechanisms and consequences of macromolecular phase separation. Cell *165*, 1067-1079.

Brangwynne, C.P., Eckmann, C.R., Courson, D.S., Rybarska, A., Hoege, C., Gharakhani, J., Julicher, F., and Hyman, A.A. (2009). Germline P granules are liquid droplets that localize by controlled dissolution/condensation. Science *324*, 1729-1732.

Breitwieser, W., Markussen, F.H., Horstmann, H., and Ephrussi, A. (1996). Oskar protein interaction with Vasa represents an essential step in polar granule assembly. Genes Dev. *10*, 2179-2188.

335 Buchan, J.R. (2014). mRNP granules. Assembly, function, and connections with disease.
336 RNA Biol *11*, 1019-1030.

337 Campbell, A.C., and Updike, D.L. (2015). CSR-1 and P granules suppress sperm-specific
338 transcription in the *C. elegans* germline. Development *142*, 1745-1755.

339 Carroll, J.S., Munchel, S.E., and Weis, K. (2011). The DExD/H box ATPase Dhh1 functions
340 in translational repression, mRNA decay, and processing body dynamics. J. Cell Biol. *194*, 527-
341 537.

342 Coller, J., and Wickens, M. (2002). Tethered function assays using 3' untranslated regions.
343 Methods *26*, 142-150.

344 Decker, C.J., and Parker, R. (2012). P-bodies and stress granules: possible roles in the
345 control of translation and mRNA degradation. Cold Spring Harb Perspect Biol *4*, a012286.

346 Decker, C.J., Teixeira, D., and Parker, R. (2007). Edc3p and a glutamine/asparagine-rich
347 domain of Lsm4p function in processing body assembly in *Saccharomyces cerevisiae*. J. Cell
348 Biol. *179*, 437-449.

349 Fowler, D.M., Koulov, A.V., Alory-Jost, C., Marks, M.S., Balch, W.E., and Kelly, J.W. (2006).
350 Functional amyloid formation within mammalian tissue. PLoS Biol. *4*, e6.

351 Hanazawa, M., Yonetani, M., and Sugimoto, A. (2011). PGL proteins self associate and bind
352 RNPs to mediate germ granule assembly in *C. elegans*. J. Cell Biol. *192*, 929-937.

353 Hoogstrate, S.W., Volkers, R.J., Sterken, M.G., Kammenga, J.E., and Snoek, L.B. (2014).
354 Nematode endogenous small RNA pathways. Worm *3*, e28234.

355 Hubstenberger, A., Courel, M., Benard, M., Souquere, S., Ernoult-Lange, M., Chouaib, R., Yi,
356 Z., Morlot, J.B., Munier, A., Fradet, M.*, et al.* (2017). P-body purification reveals the
357 condensation of repressed mRNA regulons. Mol. Cell *68*, 144-157 e145.

358 Hyman, A.A., Weber, C.A., and Julicher, F. (2014). Liquid-liquid phase separation in biology.
359 Annu. Rev. Cell. Dev. Biol. *30*, 39-58.

Jeske, M., Bordi, M., Glatt, S., Muller, S., Rybin, V., Muller, C.W., and Ephrussi, A. (2015). The crystal structure of the *Drosophila* germline inducer Oskar identifies two domains with distinct Vasa helicase- and RNA-binding activities. Cell Rep *12*, 587-598.

Kawasaki, I., Amiri, A., Fan, Y., Meyer, N., Dunkelbarger, S., Motohashi, T., Karashima, T., Bossinger, O., and Strome, S. (2004). The PGL family proteins associate with germ granules and function redundantly in *Caenorhabditis elegans* germline development. Genetics *167*, 645-661.

Kawasaki, I., Shim, Y.-H., Kirchner, J., Kaminker, J., Wood, W.B., and Strome, S. (1998). PGL-1, a predicted RNA-binding component of germ granules, is essential for fertility in *C. elegans*. Cell *94*, 635-645.

Keppler, A., Gendreizig, S., Gronemeyer, T., Pick, H., Vogel, H., and Johnsson, K. (2003). A general method for the covalent labeling of fusion proteins with small molecules *in vivo*. Nat. Biotechnol. *21*, 86-89.

Knutson, A.K., Egelhofer, T., Rechtsteiner, A., and Strome, S. (2017). Germ granules prevent accumulation of somatic transcripts in the adult *Caenorhabditis elegans* germline. Genetics *206*, 163-178.

Kortemme, T., Kim, D.E., and Baker, D. (2004). Computational alanine scanning of protein-protein interfaces. Sci STKE *2004*, pl2.

Kuznicki, K.A., Smith, P.A., Leung-Chiu, W.M.A., Estevez, A.O., Scott, H.C., and Bennett, K.L. (2000). Combinatorial RNA interference indicates GLH-4 can compensate for GLH- 1; these two P granule components are critical for fertility in *C. elegans*. Development *127*, 2907-2916.

Lee, C., Sorensen, E.B., Lynch, T.R., and Kimble, J. (2016). *C. elegans* GLP-1/Notch activates transcription in a probability gradient across the germline stem cell pool. Elife *5*, e18370.

385 Ling, S.H., Decker, C.J., Walsh, M.A., She, M., Parker, R., and Song, H. (2008). Crystal
386 structure of human Edc3 and its functional implications. Mol. Cell. Biol. *28*, 5965-5976.
387 Magis, C., Taly, J.F., Bussotti, G., Chang, J.M., Di Tommaso, P., Erb, I., Espinosa-Carrasco,
388 J., and Notredame, C. (2014). T-Coffee: Tree-based consistency objective function for
389 alignment evaluation. Methods Mol. Biol. *1079*, 117-129.
390 Maji, S.K., Perrin, M.H., Sawaya, M.R., Jessberger, S., Vadodaria, K., Rissman, R.A., Singru,
391 P.S., Nilsson, K.P., Simon, R., Schubert, D.*, et al.* (2009). Functional amyloids as natural
392 storage of peptide hormones in pituitary secretory granules. Science *325*, 328-332.
393 Markussen, F.H., Michon, A.M., Breitwieser, W., and Ephrussi, A. (1995). Translational
394 control of *oskar* generates Short OSK, the isoform that induces pole plasma assembly.
395 Development *121*, 3723-3732.
396 Nott, T.J., Petsalaki, E., Farber, P., Jervis, D., Fussner, E., Plochowietz, A., Craggs, T.D.,
397 Bazett-Jones, D.P., Pawson, T., Forman-Kay, J.D.*, et al.* (2015). Phase transition of a
398 disordered nuage protein generates environmentally responsive membraneless organelles. Mol.
399 Cell *57*, 936-947.
400 Paix, A., Folkmann, A., Rasoloson, D., and Seydoux, G. (2015). High efficiency, homology-
401 directed genome editing in *Caenorhabditis elegans* using CRISPR-Cas9 ribonucleoprotein
402 complexes. Genetics *201*, 47-54.
403 Saha, S., Weber, C.A., Nousch, M., Adame-Arana, O., Hoege, C., Hein, M.Y., Osborne-
404 Nishimura, E., Mahamid, J., Jahnel, M., Jawerth, L.*, et al.* (2016). Polar positioning of phase-
405 separated liquid compartments in cells regulated by an mRNA competition mechanism. Cell
406 *166*, 1572-1584 e1516.
407 Schisa, J.A., Pitt, J.N., and Priess, J.R. (2001). Analysis of RNA associated with P granules
408 in germ cells of *C. elegans* adults. Development *128*, 1287-1298.
409 Singh, G., Pratt, G., Yeo, G.W., and Moore, M.J. (2015). The clothes make the mRNA: past
410 and present trends in mRNP fashion. Annu. Rev. Biochem. *84*, 325-354.

411 Spike, C., Meyer, N., Racen, E., Orsborn, A., Kirchner, J., Kuznicki, K., Yee, C., Bennett, K.,
412 and Strome, S. (2008). Genetic analysis of the *Caenorhabditis elegans* GLH family of P-granule
413 proteins. Genetics *178*, 1973-1987.

414 Strome, S., and Updike, D. (2015). Specifying and protecting germ cell fate. Nat. Rev. Mol.
415 Cell Biol. *16*, 406-416.

416 Tang, W., Tu, S., Lee, H.C., Weng, Z., and Mello, C.C. (2016). The RNase PARN-1 trims
417 piRNA 3' ends to promote transcriptome surveillance in *C. elegans*. Cell *164*, 974-984.

418 Updike, D., and Strome, S. (2010). P granule assembly and function in *Caenorhabditis*
419 *elegans* germ cells. J Androl *31*, 53-60.

420 Updike, D.L., Hachey, S.J., Kreher, J., and Strome, S. (2011). P granules extend the nuclear
421 pore complex environment in the *C. elegans* germ line. J. Cell Biol. *192*, 939-948.

422 Updike, D.L., Knutson, A.K., Egelhofer, T.A., Campbell, A.C., and Strome, S. (2014). Germ-
423 granule components prevent somatic development in the *C. elegans* germline. Curr. Biol. *24*,
424 970-975.

425 Vanzo, N.F., and Ephrussi, A. (2002). Oskar anchoring restricts pole plasm formation to the
426 posterior of the *Drosophila* oocyte. Development *129*, 3705-3714.

427 Voronina, E., Paix, A., and Seydoux, G. (2012). The P granule component PGL-1 promotes
428 the localization and silencing activity of the PUF protein FBF-2 in germline stem cells.
429 Development *139*, 3732-3740.

430 Voronina, E., Seydoux, G., Sassone-Corsi, P., and Nagamori, I. (2011). RNA granules in
431 germ cells. Cold Spring Harb Perspect Biol *3*, a002774.

432 Wang, J.T., Smith, J., Chen, B.C., Schmidt, H., Rasoloson, D., Paix, A., Lambrus, B.G.,
433 Calidas, D., Betzig, E., and Seydoux, G. (2014). Regulation of RNA granule dynamics by
434 phosphorylation of serine-rich, intrinsically disordered proteins in *C. elegans*. Elife *3*, e04591.

435 Wedeles, C.J., Wu, M.Z., and Claycomb, J.M. (2013). Protection of germline gene
436 expression by the *C. elegans* Argonaute CSR-1. Dev. Cell *27*, 664-671.

437 Wippich, F., Bodenmiller, B., Trajkovska, M.G., Wanka, S., Aebersold, R., and Pelkmans, L.
438 (2013). Dual specificity kinase DYRK3 couples stress granule condensation/dissolution to
439 mTORC1 signaling. Cell *152*, 791-805.

440 Wu, H., and Fuxreiter, M. (2016). The structure and dynamics of higher-order assemblies:
441 amyloids, signalosomes, and granules. Cell *165*, 1055-1066.

442 Zeiser, E., Frøkjær-Jensen, C., Jorgensen, E., and Ahringer, J. (2011). MosSCI and gateway
443 compatible plasmid toolkit for constitutive and inducible expression of transgenes in the *C.*
444 *elegans* germline. PLoS One *6*, e20082.

445

446

447 **Figure Legends**

448 **Figure 1**. Crystal structure of the PGL NTD

449 (A) Left, *C. elegans* adult hermaphrodite possesses two gonadal arms with proliferating germ
450 cells at one end (asterisk) and differentiating gametes at the other. Gonads make sperm (blue)
451 first and then oocytes (pink). Right, P-granules (magenta) reside at the nuclear periphery of all
452 germ cells until late oogenesis. (B) Linear diagram of *C. elegans* PGL-1. (C) Crystal structure of
453 *C. japonica* PGL-1 NTD to 1.5 Å. NTD has four copies per asymmetric unit (ASU). Copies in
454 yellow, gold, tan, and brown. Arrows indicate two pairs of subunit interfaces in the ASU. Red
455 arrows highlight the interface relying on conserved amino acids (see text). (D) Enlarged image
456 of a single NTD.

457

458 **Figure 2**. NTD dimerization and its role in PGL self-assembly

459 (A) Structural model of the NTD dimer. (B-C) Enlargement of dimer interface (red box in A).
460 PGL-1 K126 and K129 (B), and R123 (C) interact with apposing subunit side chains. Residue
461 labels in yellow or gold to indicate their representative subunits. (D-E) Size exclusion
462 chromatography and multi-angle light scattering (SEC-MALS) of recombinant PGL-3 NTD wild
463 type (D-E), K126E K129E (D) and R123E (E) proteins. A280 UV absorbance (left y axis) was
464 normalized to the maximum value. Molecular weight (MW, right y axis) for MALS in daltons
465 (Da). Wild-type protein (blue) measured the approximate size of a dimer, while both mutant
466 proteins (red) measured approximately as monomers. (F) Diagram of *C. elegans* PGL-1 C-
467 terminally tagged with GFP. (G-J). Representative images of GFP-tagged PGL-1 (G), GFP
468 alone (H), and GFP-tagged PGL-1 K126E K129E (I) and R123E (J) mutants expressed in
469 Chinese Hamster Ovary (CHO) cells. Cell cultures were imaged live, and GFP-positive cells
470 counted for the presence or absence of granules. Images show the majority result (percentages
471 noted above image). Scale bar, 10 μm.

472

Figure 3. NTD dimerization is critical for fertility and P-granule formation in nematodes

(A) Site of SNAP tag insertion in *C. elegans* PGL-1. (B) Fertility of SNAP tagged PGL-1 animals. Percentages were obtained after scoring individuals for production of larval progeny after 5 days at either 20°C or 25°C. (C-P) Extruded adult germlines, fixed, stained and imaged in same region of meiotic pachytene (see **Figure S3A**). (C-F) Representative images of SNAP staining to visualize PGL-1 expression and granule formation. All images are partial z-stacks to maximize visualization of P-granules. Images were taken from germlines producing embryos; similar images were obtained from germlines too defective to make embryos (**Figure S3F-G**). (C) Control, wild type animal lacking SNAP tag shows virtually no background staining (n=20). (D) PGL-1::SNAP localizes to granules around nuclei (n=49). (E) PGL-1::SNAP K126E K129E is diffuse (n=38). (F) PGL-1::SNAP R123E is diffuse (n=24). (G-P) Representative images showing localization of three P-granule components in germ cells expressing either PGL-1::SNAP (G-K, n=20) or PGL-1::SNAP K126E K129E (L-P, n=14). (G,L) DNA (DAPI); (H,M) SNAP (PGL-1::SNAP or mutant); (I,N) V5 (PGL-3); (J,O) MYC (GLH-1); (K,P) Merge. Scale bar, 10 μm for all images, except two-fold enlargements of nuclei in white boxes that are placed outside main images.

Figure 4. PGL assembly is required for repression of tethered mRNA reporter *in vivo*

(A) Tethering assay. The reporter mRNA encodes GFP-histone H2B and harbors three boxb hairpins in its 3'UTR; a ubiquitous germline promoter drives expression (see Methods). λN22 peptide (light blue) is inserted into PGL-1::SNAP. Binding of PGL-1::SNAP::λN22 to boxB hairpins recruits PGL-1 to reporter mRNA. (B-D) GFP reporter expression in germ cells of live animals. Above, brightfield image; below GFP fluorescence (green); auto fluorescence (red). n, number of animals scored for GFP expression. Scale bar, 10 μm, in (B) applies to all images. (E-G) Representative images of PGL granule formation, seen by SNAP staining (magenta), and GFP fluorescence (green) in fixed gonads. n, number of germlines scored for GFP expression.

499 Scale bar, 10 μm, in (E) applies to all images. (H) Model of P-granule assembly and function.
500 Left, NTD dimerization allows PGL granule formation, which traps and represses mRNA
501 transcripts. Right, loss of PGL granule formation derepresses granule-localized mRNA
502 transcripts. See text for further Discussion.
503
504

505 **Supplemental Figure Captions**

506

507 **Table S1**. *C. japonica* PGL-1 NTD crystal structure data and model statistics

508

509 **Figure S1**. PGL sequence alignment and locus

510 (A) Sequence alignment of PGL NTD domain in *C. elegans* (*Ce*), *C. japonica* (*Cj*), *C. brenneri*
511 (*Cbn*), *C. briggsae* (*Cbr*), *C. remanei* (*Cr*). Alignment and conservation (cons.) determined by T-
512 Coffee (Magis et al., 2014). Starred residues (*) are identical. Period (.) and colon (:) residues
513 are similar. Residues participating in salt bridges only are in orange. Residues participating in
514 hydrogen bonds only are in yellow. Residues forming both hydrogen bonds and salt bridges are
515 highlighted in red. *C. elegans* PGL-1 missense mutations and their allele numbers are labeled.
516 Dashed lines mark the end of PGL-1 NTD domain and start of PGL-1 DD domain. (B) *pgl-1*
517 (ZK481.4a.1) primary transcript. 5' and 3' UTRs are grey, exons are white, numbered 1-8 and
518 separated by introns. Sites of *pgl-1* mutations are labeled, including location of SNAP tag
519 (magenta) and λN22 fusion (blue).

520

521 **Figure S2**. Supplemental biochemical and structural analyses of PGL NTD

522 (A,B) Coomassie-stained polyacrylamide gel of recombinant PGL NTD wild type and mutant
523 protein. Ladder marker sizes labeled in kilodaltons (kDa) on right. (A) Recombinant *C. japonica*
524 (Cj) PGL-1 NTD protein used for crystallization. Recombinant *C. elegans* PGL-3 NTD protein
525 included for comparison. (B) Wild type and mutant *C. elegans* PGL-3 NTD recombinant proteins
526 used for biochemical characterization. (C) Tables of predicted hydrogen bonds and salt bridges
527 at the NTD dimerization interface. Amino acid numbers correspond to *C. japonica* PGL-1 NTD.
528 (D-E) Surface representation of the NTD dimerization interface. (D) Amino acids colored by
529 identity (red) and similarity (pink). (E) Amino acids at dimerization interface (purple).

530

Figure S3. Supplemental images of PGL-1 dimerization mutants

(A) Schematic of an adult hermaphrodite germline. An asterisk marks proliferating germ cells here and in images B-D. The germline produces oocytes at this stage; sperm were made earlier and stored in the spermatheca (not shown). Red box marks region imaged in F-I. (B-D) Representative brightfield images of extruded gonads from worms grown at 20°C. Scale bar, 10 µm. (B) PGL-1::SNAP gonads are of normal size and produce oocytes and embryos. (C) Representative images of PGL-1::SNAP K126E K129E sterile gonads, which are small and produce no gametes. (D) PGL-1::SNAP R123E sterile gonads are also small and produce no gametes. (F-I) Representative partial z-projection stacks of SNAP and DNA stained germlines. Scale bar, 10 µm, applies for all images. (F,G) PGL-1 is expressed in sterile gonads (no embryos observed). (F) n=21 gonads imaged; (G) n=30 gonads imaged. (H-I) In single rare gonads, PGL-1 mutants were seen to assemble into granules in all germ cells. Note the diffuse staining between nuclei, which is not seen in the wild-type PGL-1::SNAP (see **Figure 3D**).

Figure S4. GFP reporter is not subject to germline silencing

Gonads were extruded from animals harboring (A-D) PGL-1::SNAP (n=30); (E-H,M) PGL-1::SNAP::λN22 (n=27); (I-L) PGL-1::SNAP::λN22 K126E K129E (n=10). Gonads were fixed and imaged for *gfp* RNA using smFISH (A,E,I), GFP protein fluorescence (B,F,J), DNA (DAPI) and SNAP (C,G,K). The three are merged in D, H, L, and M. White arrows mark examples of intranuclear puncta; black arrows mark examples of cytoplasmic puncta. (I) Six additional examples of germlines harboring PGL-1::SNAP::λN22, imaged for *gfp* RNA, DNA, and SNAP. Scale bar, 5 µm, for all images, except image in inset (white box) enlarged 2.5-fold. For germline location, see **Figure S3A**.

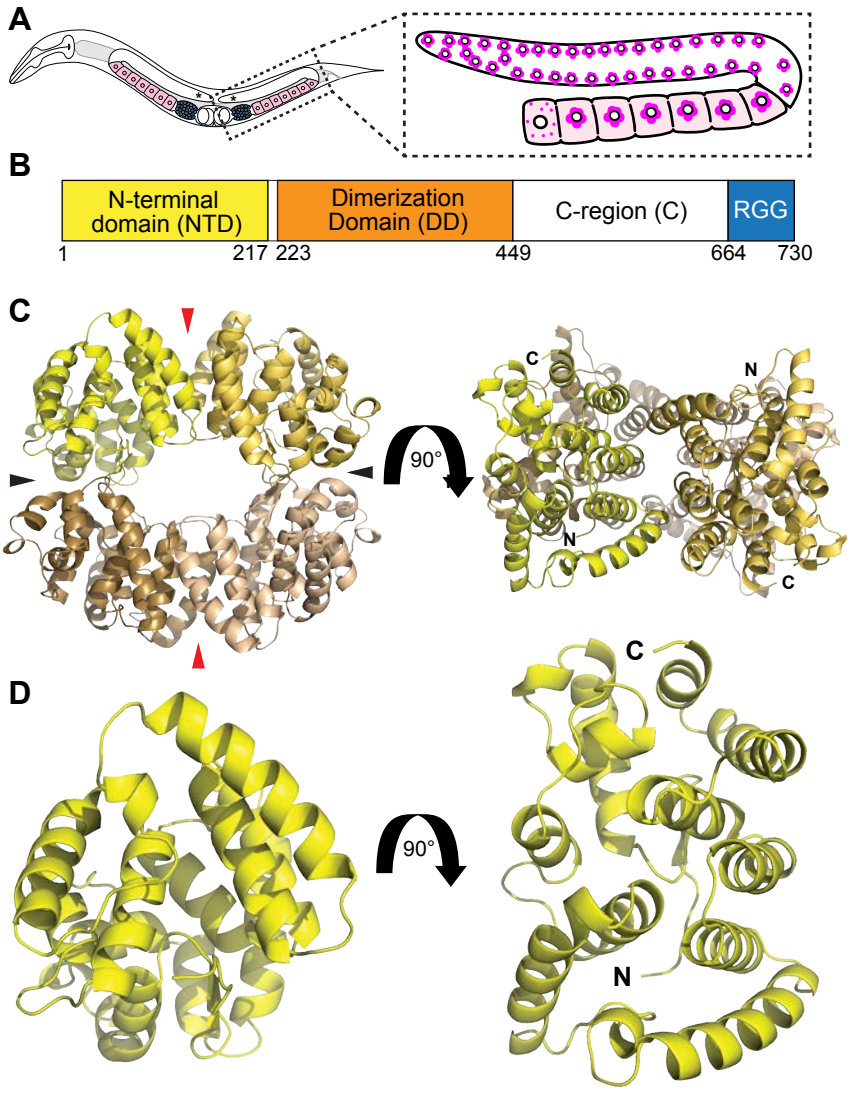

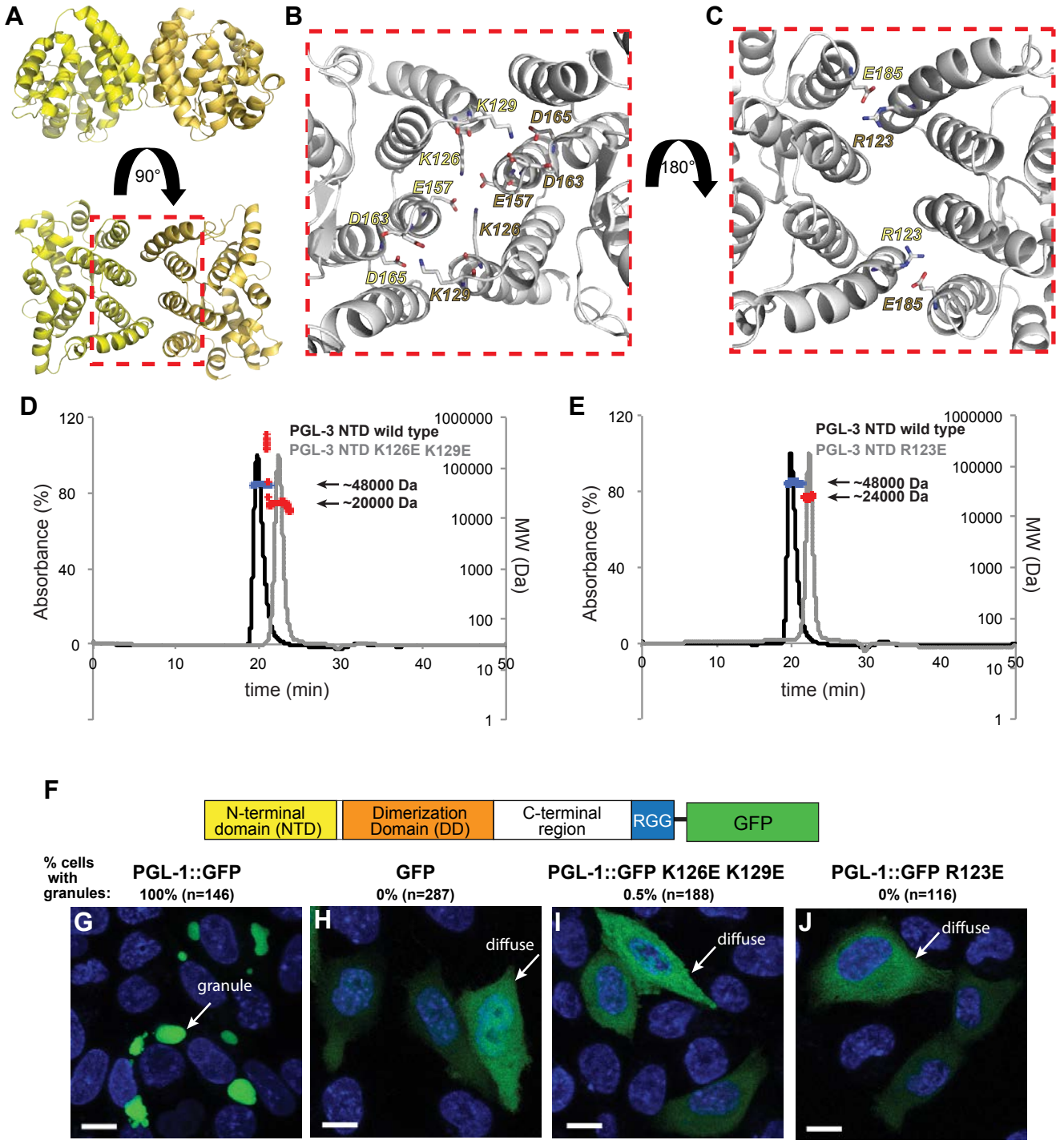

A

B

Protein	allele	20°C % sterile	20°C n	25°C % sterile	25°C n
PGL-1	N2	1.0	96	2.2	93
PGL-1::SNAP	*q894*	1.1	93	8.6	93
PGL-1 null	*bn102*	3.3	92	82.3	96
PGL-1::SNAP K126E K129E	*q960*	72.0	93	100	92
PGL-1::SNAP R123E	*q975*	22.1	95	97.9	96

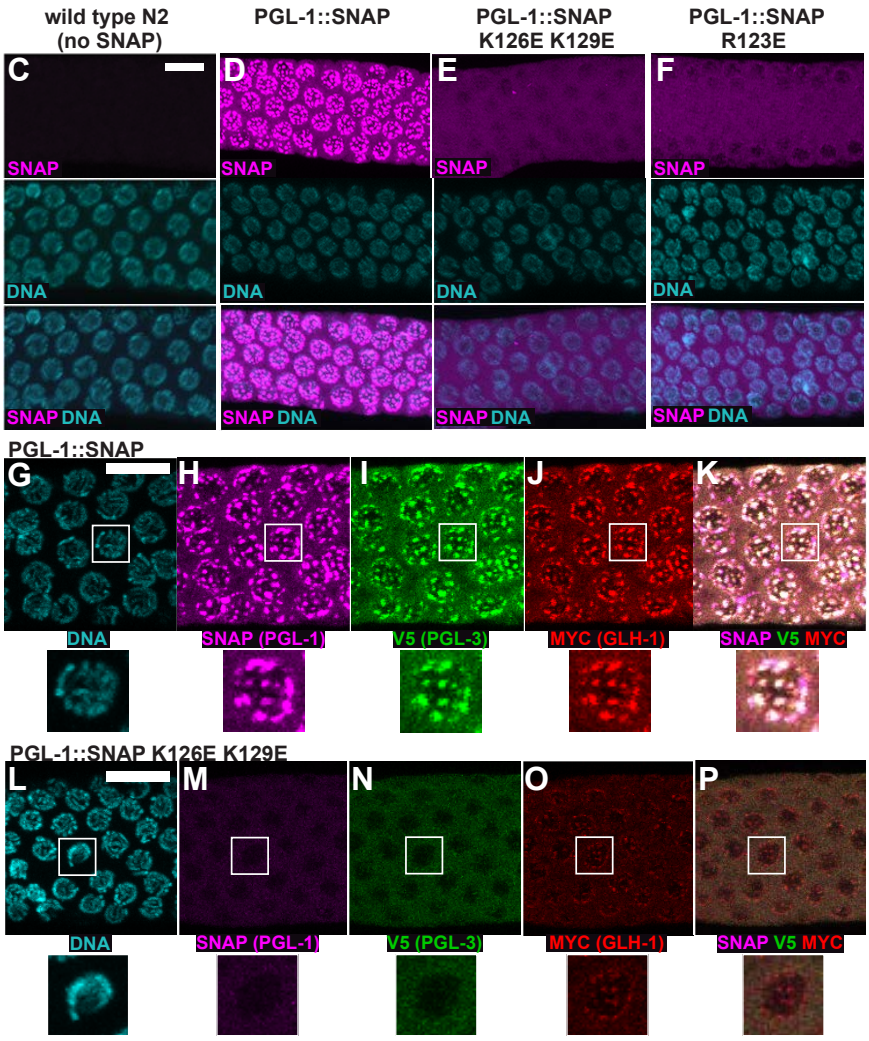

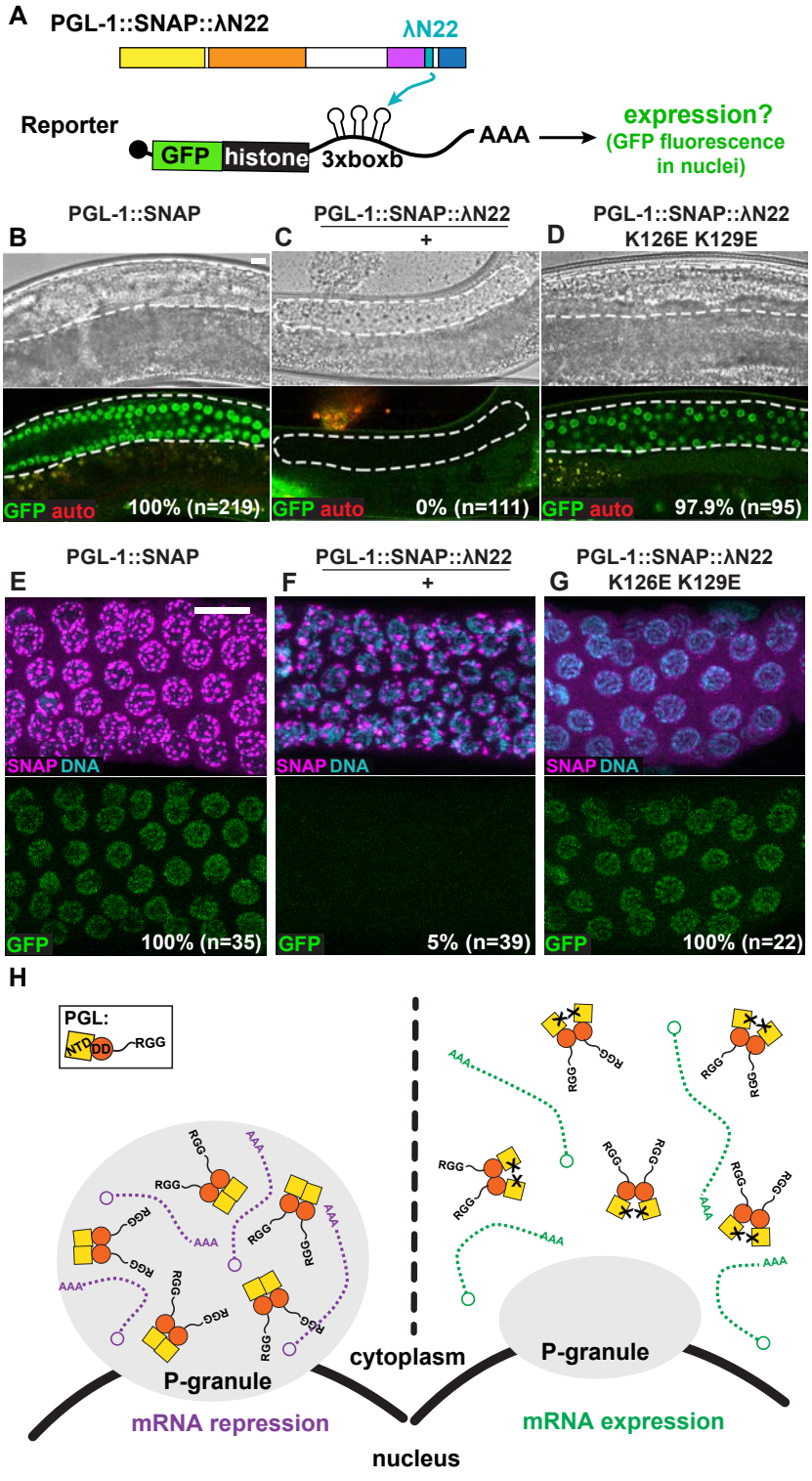

Table S1. Data collection and refinement statistics.

	JaPGL-1N SeMet (5W4D)	JaPGL-1N wt (5W4A)
Wavelength	0.9786	0.984
Resolution range	48.47 - 1.599 (1.656 - 1.599)	30.36 - 1.5 (1.554 - 1.5)
Space group	C 1 2 1	C 1 2 1
Unit cell	133.3 94.8 72.5 90 91.4 90	132.77 94.67 72.95 90 90.756 90
Total reflections	880332 (81451)	2176741 (194944)
Unique reflections	115340 (11239)	143729 (14301)
Multiplicity	7.6 (7.2)	15.1 (13.6)
Completeness (%)	97.06 (95.16)	99.77 (99.33)
Mean I/sigma(I)	24.44 (2.30)	16.91 (1.85)
Wilson B-factor	22.04	22.44
R-merge	0.0469 (0.8775)	0.08108 (1.282)
R-meas	0.05038 (0.945)	0.08353 (1.332)
R-pim	0.01827 (0.348)	0.01984 (0.357)
CC1/2	0.999 (0.74)	0.997 (0.662)
CC*	1 (0.922)	0.999 (0.893)
Reflections used in refinement	115302 (11238)	143649 (14297)
Reflections used for R-free	1424 (129)	1468 (151)
R-work	0.1607 (0.2590)	0.1681 (0.3038)
R-free	0.1925 (0.2707)	0.2039 (0.3232)
CC(work)	0.962 (0.864)	0.967 (0.802)
CC(free)	0.939 (0.819)	0.974 (0.794)
Number of non-hydrogen atoms	7593	7785
macromolecules	6768	6813
ligands	168	136

solvent	657	836
Protein residues	846	853
RMS(bonds)	0.010	0.010
RMS(angles)	1.00	0.99
Ramachandran favored (%)	98.68	98.10
Ramachandran allowed (%)	1.32	1.90
Ramachandran outliers (%)	0.00	0.00
Rotamer outliers (%)	1.33	0.66
Clashscore	2.29	1.86
Average B-factor	30.58	30.21
macromolecules	29.29	28.97
ligands	53.64	51.75
solvent	37.95	36.82
Number of TLS groups	1	1

Statistics for the highest-resolution shell are shown in parentheses.

Figure S1
Aoki, et al.

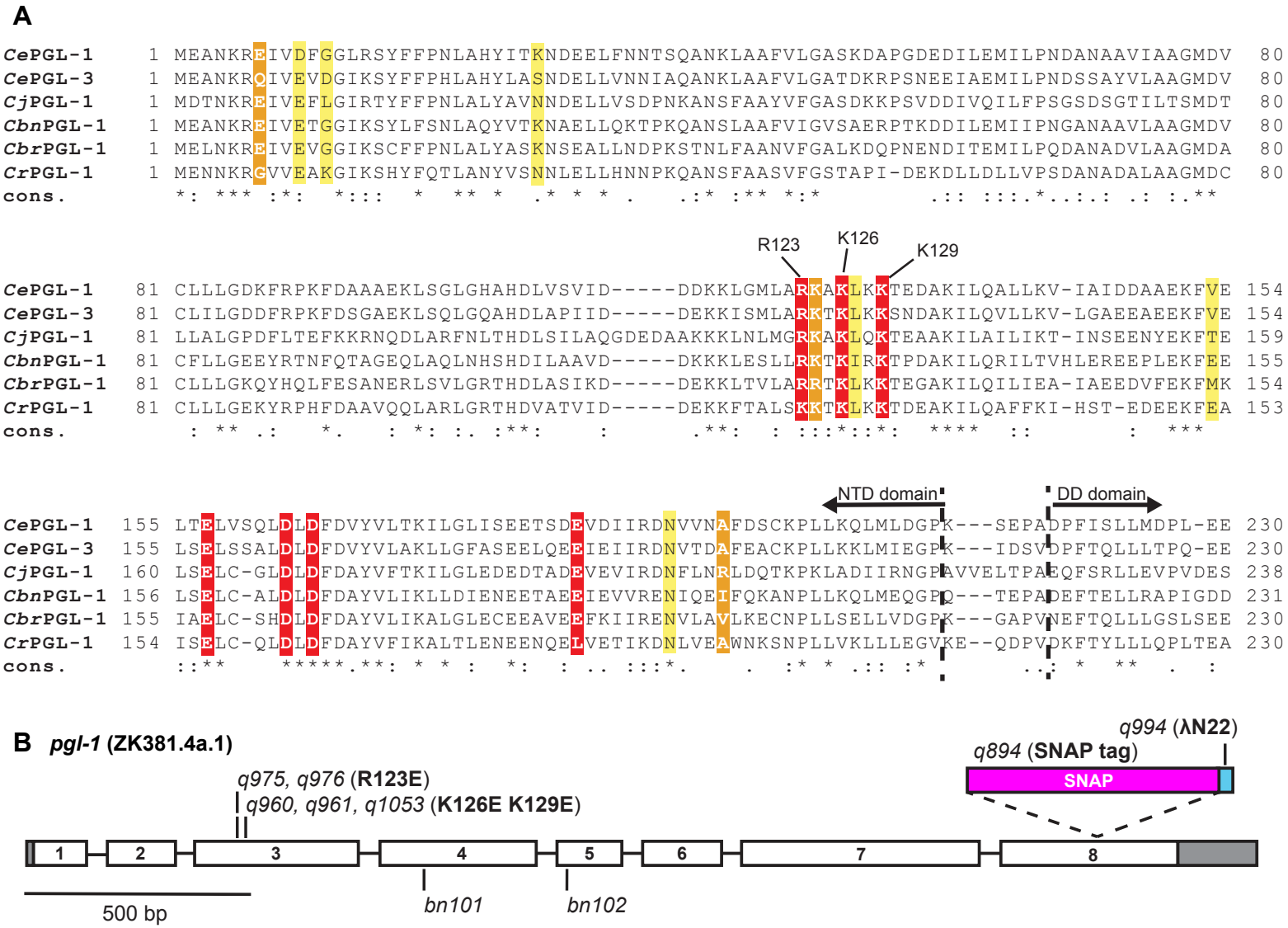

A

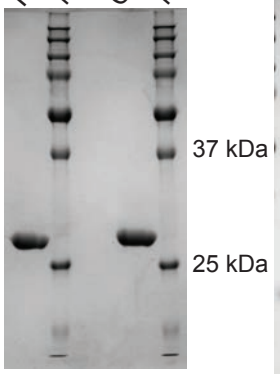

B

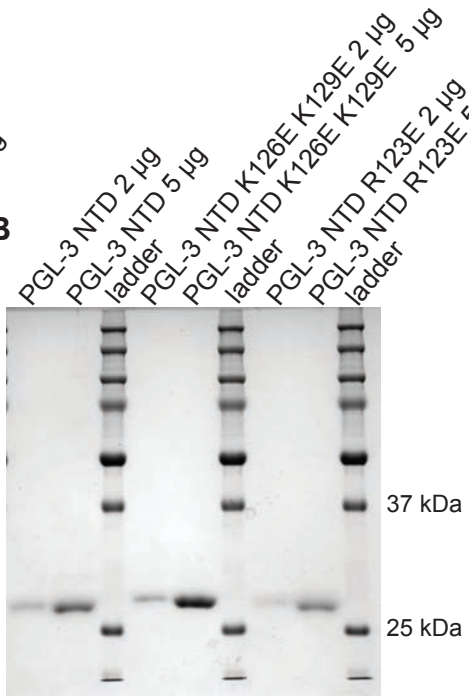

C

H-bonds

subunit 1	subunit 2
A:R128	B:T158
A:R128	B:E189
A:K131	B:E162
A:L132	B:N196
A:K134	B:D167
A:K134	B:D169
A:T158	B:R128
A:E162	B:K131
A:D167	B:K134
A:D169	B:K134
A:E189	B:R128
A:N196	B:L132

salt bridges

subunit 1	subunit 2
A:R128	B:E189
A:K131	B:E162
A:K134	B:D167
A:K134	B:D169
A:E162	B:K131
A:D167	B:K134
A:D169	B:K134
A:E189	B:R128

D

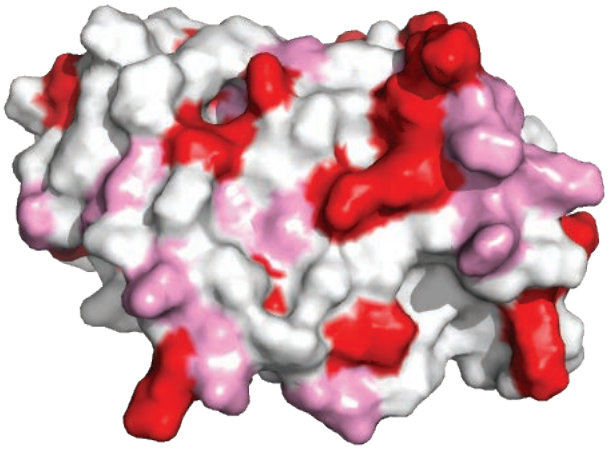

E

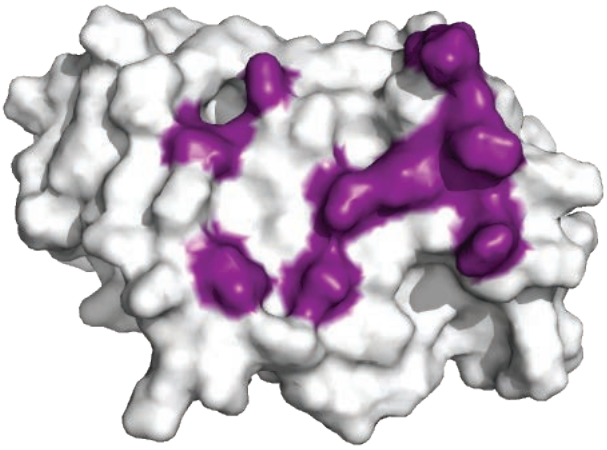

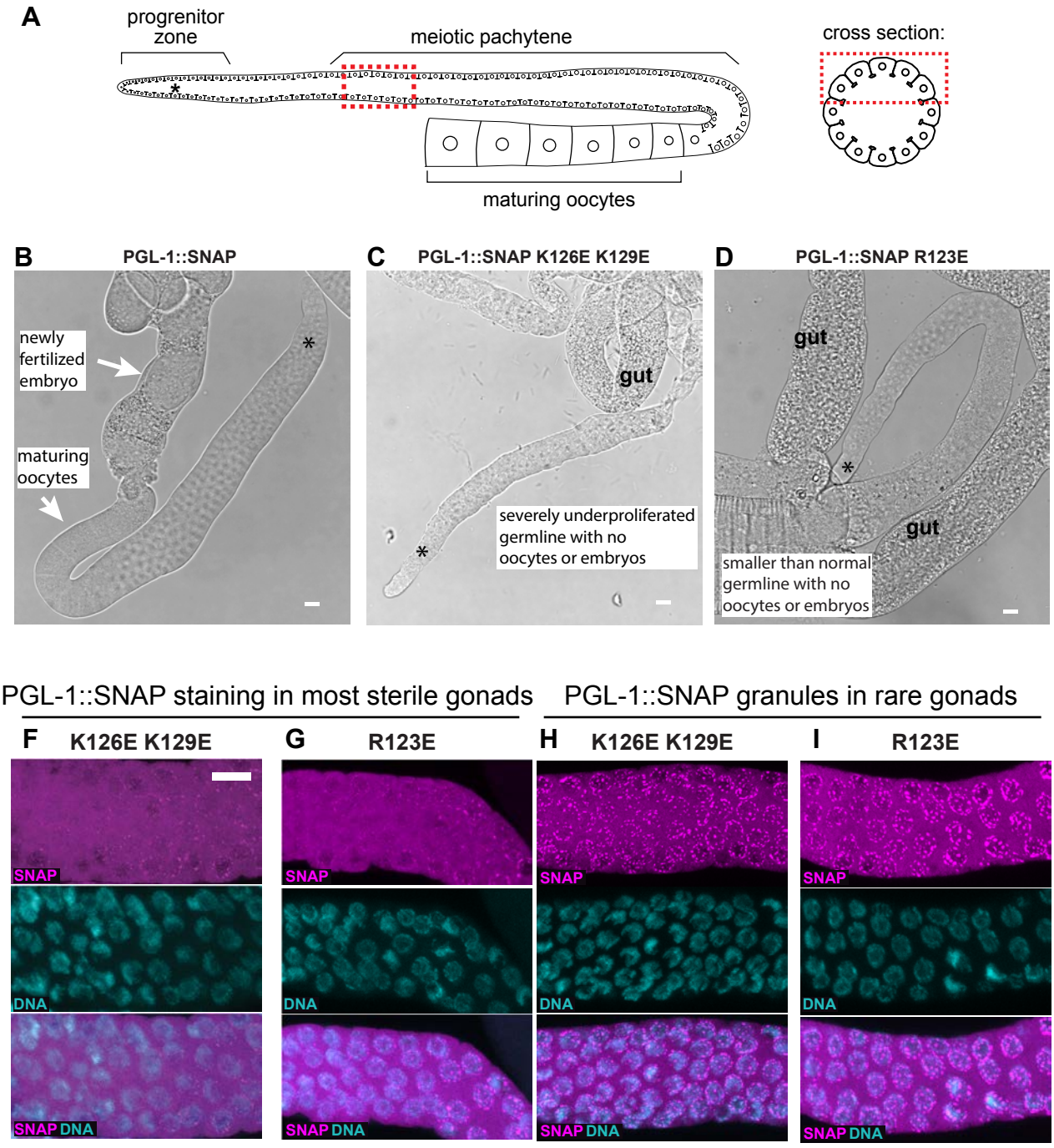

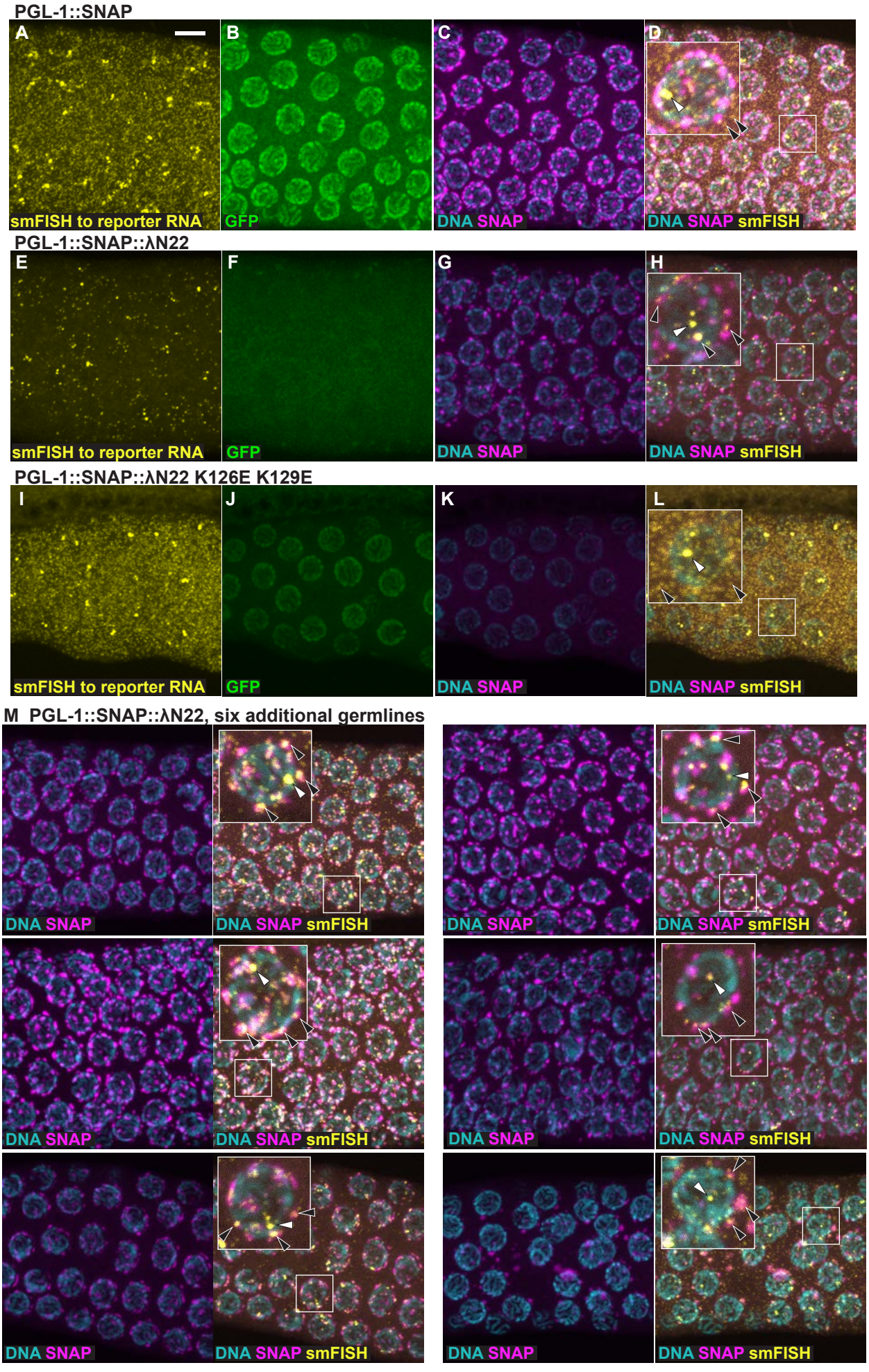

Materials and Methods

Protein expression and purification

We previously used *C. elegans* PGL-3 recombinant protein and limited proteolysis to identify a central dimerization domain (DD) (Aoki et al., 2016). While we could express DD efficiently we could not express recombinant protein that was N-terminal to the cleavage site (PGL-3 amino acid residues 205-206). We tried moving the six histidine purification tag to the N- and C- termini, shortened the protein regions used for expression, and tried several different orthologs with little success. The insight came after aligning protein sequences of several *Caenorhabditid sp.* and studying the DD domain boundary (**Figure S1A**). Protease cleavage occurred in a conserved portion of the N-terminal region and this region was disordered in our DD crystal structures. After inclusion of this region (PGL-3 amino acid residues 205-212), we could express and purify recombinant N-terminal protein from *C. elegans* PGL-1 and its orthologs. We henceforth refer to this region as the N-terminal domain (NTD).

This study used primarily *C. elegans* PGL-3 and *C. japonica* PGL-1 recombinant NTD proteins. The *C. elegans* PGL-3 coding region was PCR amplified from cDNA. A codon-optimized (*E. coli*) version of *C. japonica* PGL-1 NTD was ordered as a gBlock (IDT). We included a six-histidine tag at the C-terminus that was removed later with carboxypeptidase A (Arnau et al., 2006). Constructs were cloned into a pET21a vector (Merck-Millipore) with Gibson Assembly cloning (Gibson, 2011), and plasmids transformed into Rosetta2 cells (EMD-Millipore). Cultures were grown at 37°C with shaking (225 rpm) until ~0.8 OD, cooled for 30-60 minutes, and induced with a final concentration of 0.1 mM IPTG. Cultures were then grown at 16°C with shaking (160 rpm) for 16-18 hours, collected, and bacterial pellets frozen until use. Selenomethionine-incorporated *C. japonica* protein was expressed in SelenoMethionine Medium Complete (Molecular Dimensions), and grown, induced, and collected in a similar manner.

Bacterial pellets were defrosted on ice and reconstituted in lysis buffer (20 mM Sodium Phosphate pH 7.4, 300 mM NaCl, 10 mM imidazole, 5 mM beta-mercaptoethanol (BME)) with protease inhibitors (cOmplete™ EDTA-free, Roche). Lysozyme was added at 50 µg/ml and incubated on ice for 20 minutes prior to lysis in a french press. Samples were spun at low (3220 x g, 4°C, 20 minutes) and high speed

(10,000 x g, 20°C, 10 minutes), then incubated with 1.5 ml NiNTA beads (Thermo Scientific) for 1 hour at 4°C with rotation. Sample supernatant was separated by gravity flow, washed twice with lysis buffer, and eluted using lysis buffer with increasing imidazole concentrations (20, 40, 60, 80, 100, 250 mM). Eluted samples were checked for protein via Bradford assay (Bio-Rad), and dialyzed overnight in HN buffer (20 mM HEPES pH 7.4, 100 mM NaCl). The dialyzed samples were concentrated with a Centriprep 10K concentrator (Millipore), calcium added to 1 mM $CaCl_2$, and the histidine tag removed with carboxypeptidase A bound to agarose (Sigma) at a ratio of 10 protein:1 enzyme (w/w). Samples were incubated at room temperature (~20°C) for 45-90 minutes with rotation prior to supernatant elution by centrifugation in microflow columns (Pierce). Samples were run on a S200 sizing column (GE Healthcare) in HNT buffer (20 mM HEPES pH 7.4, 100 mM NaCl, 0.5 mM TCEP pH 7.4). Fractions containing recombinant protein were collected, concentrated in an Amicon 10K concentrator (Millipore), and protein concentration estimated by A280. Samples were frozen in liquid nitrogen or used immediately.

Crystallization and structure determination

C. elegans PGL-1, *C. elegans* PGL-3, and *C. japonica* PGL-1 NTD recombinant protein were screened in crystallization conditions using 400 nl hanging and sitting drop 96-well trays set up with the Mosquito (TTP Labtech) in 20°C. Several conditions produced labile crystal plates. Data was collected to 4 Å from *C. elegans* PGL-1 crystal plates, determined to have a very large unit cell (86 Å x 86 Å x 460 Å) and P6 point group, and eventually determined to have perfect merohedral twinning. *C. japonica* PGL-1 also crystallized as large (60-150 Å) rhomboid crystals in 40-45% PEG 400 at low (Na Citrate pH 5.5-6.0) and physiologic pH (imidazole pH 7.5-8.0). Crystals grown in citrate or imidazole both diffracted well, but we used imidazole (100 mM imidazole pH 7.5, 45% PEG 400, 1 mM TCEP pH 7.4) due to its higher reproducibility for large crystals and its modestly better resolution. The crystals did not require additional cryo-protection due to the high PEG 400. We eventually collected a full data set to 1.5 Å in space group C2.

PGL-1 NTD was a novel domain. Novelty and translational pseudosymmetry precluded us from using any model for molecular replacement. Trial heavy atom soaks also proved unfruitful, and the *C. japonica* PGL-

1 NTD has just two methonines past the start codon, making selenomethionine phasing challenging. To boost anomalous signal, we mutated two non-conserved isoleucines to methionines (I63M, I212M). This methionine mutant provided phases to 3.6 Å by single anomalous dispersion (SAD) that we used to build a 1.6 Å model of the mutant protein (PDB ID: **5W4D**). We used this model for molecular replacement into the wild-type data set to build a complete 1.5 Å model (PDB ID: **5W4A**). Data and model statistics are in Supplemental Table 1. Model coordinates and data are available at RCSB (www.rcsb.org).

Size exclusion chromatography with multi-angle laser light scattering (SEC-MALS)

Molecular weights of *C. elegans* PGL-3 NTD wild type and mutant recombinant protein were determined by conducting SEC-MALS experiments using Agilent Technologies 1260 LC HPLS system (Agilent Technologies) equipped with Dawn® Heleos™II 18-angle MALS light scattering detector, Optilab® T-rEX™ (refractometer with EXtended range) refractive index detector, WyattQELS™ quasi-elastic (dynamic) light scattering (QELS) detector and ASTRA software (all four from Wyatt Technology Europe GmbH). A total of 500 µL (1 mg/mL) of the samples in HNT buffer (20 mM HEPES pH 7.5, 100 mM NaCl, 0.5 mM TCEP pH 7.4) were injected and run on a Superdex 75 10/300 GL column (GE Healthcare) pre-equilibrated with the same buffer, at a flow rate of 0.5 mL/min at 20°C. Lysozyme (Sigma-Aldrich Corp.) was used as a control.

Mammalian cell culture maintenance, transfection and imaging

Full length PGL-1 was cloned into a pcDNA 3.1 vector (Thermofisher) with a C-terminal eGFP and OLLAS epitope linker. Mutations to PGL-1 were created using Gibson Assembly cloning (Gibson, 2011). Chinese Hamster Ovary (CHO) cells (ATCC) were propagated according to distributor's recommendations. Briefly, cells were grown in F-12K Medium (Gibco) with 10% fetal bovine serum (Gibco), and split with Trypsin 0.25% (Gibco) every 2-3 days. Cells were grown to 70% confluence and transfected with TransIT-CHO Transfection Kit (Mirus Bio). Transfected cells were split the following day and grown in Ibitreat 15 u-Slide 8 well slides (Ibidi) overnight. Hoechst stain (Invitrogen) was added to wells prior to imaging by confocal microscopy for GFP and Hoechst fluorescence, and transmitted light. Well dilutions were chosen based on adequate cell spacing to discern each cell, and 25 fields of view

were taken based on the highest concentration of GFP-positive cells. Experiments were repeated four times with similar results. During image collection, we observed a single example of a granule-like blob in the PGL-1::OLLAS::GFP K126E K129E. The cell appeared unhealthy, and thus the granule may be an artifact of cell death, but we included it in our study for completeness.

Worm maintenance, CRISPR mutagenesis, fertility and imaging

Frozen strains:

N2 Bristol

JK5687: *pgl-1(q894)[PGL-1::SNAP] IV*

JK5902: *pgl-1(q975)[PGL-1::SNAP R123E] IV*

JK5898: *glh-1(q858)[GLH-1:: 3xMYC] I; pgl-1(q894)[PGL-1::SNAP] IV; pgl-3(q861)[PGL-3::3xV5] V*

JK5970: *qSi375[(mex-5 promoter::eGFP::linker::his-58::3xboxb::tbb-2 3'UTR) *weSi2] II; pgl-1(q894)[PGL-1::SNAP] IV*

JK5873: *qSi375[(mex-5 promoter::eGFP::linker::his-58::3xboxb::tbb-2 3'UTR) *weSi2] II; pgl-1(q994)[PGL-1:SNAP::λN22]/nT1[qIs51](IV;V)*

JK5874: *qSi375[(mex-5 promoter::eGFP::linker::his-58::3xboxb::tbb-2 3'UTR) *weSi2] II; pgl-1(q994)[PGL-1:SNAP:λN22]/nT1[qIs51](IV;V)*

Worm strains that could not be frozen:

1. *pgl-1(q960)[PGL-1::SNAP K126E K129E] IV*
2. *glh-1(q858)[GLH-1::3xMYC] I; pgl-1(q960)[PGL-1::SNAP K126E K129E] IV; pgl-3(q861)[PGL-3::3xV5] V*
3. *qSi375[(mex-5 promoter::eGFP::linker::his-58::3xboxb::tbb-2 3'UTR) *weSi2] II; pgl-1(q1053)[PGL-1:SNAP:λN22 K126E K129E]/nT1[qIs51](IV;V)*

C. elegans were maintained as previously reported (Brenner, 1974). For CRISPR-Cas9 mutagenesis, a Cas9 protein co-conversion approach was used (Arribere et al., 2014). Briefly, worms were injected with a target CRISPR-Cas9 RNA (crRNA) or a plasmid expressing a Cas9-scaffold with tandem target sequence

RNA (sgRNA) to a gene of interest (Arribere et al., 2014), a target crRNA to *dpy-10* or *unc-58*, a scaffolding tracrRNA (IDT), recombinant Cas9 protein (Paix et al., 2015), a *dpy-10/unc-58* repair DNA oligo that inserted a dominant mutation (Arribere et al., 2014), and an epitope tag/missense mutant repair oligo or PCR product. See below for a Table of guide RNAs and repair templates used. F1s with the co-injection marker phenotype were additionally screened by a combination of PCR without or with restriction enzyme digest to identify those with the repair of interest. In JK5687, a SNAP tag (Keppler et al., 2003) was inserted between PGL-1 amino acids G713 and G714 in N2 worms. A 3xMYC tag was added to the N-terminus of GLH-1 between G17 and F18. A 3xV5 tag was added in the C-terminal region of PGL-3 between residues G627 and S628. F2s were PCR screened to identify homozygous SNAP alleles and the PCR product sequenced to confirm proper repair. Three worm strains were too infertile to freeze. All worms were outcrossed at least twice with N2, with the exception of (*glh-1(q858)[GLH-1::3xMYC] I; pgl-1(q960)[PGL-1::SNAP K126E K129E] IV; pgl-3(q861)[PGL-3::3xV5] V)* that was backcrossed with JK5898.

Worms were singled into the peripheral wells of a 24-well plate that contained NGM agar and OP50 bacteria. Worms were allowed to propagate for 5 days at 20°C or 25°C, and then scored for progeny and gravid progeny. We report the progeny numbers here.

To analyze GFP reporter expression, L4 larvae were propagated for approximately 24 hours at 20°C, placed in M9 with 0.1 mM levamisole on a glass slide with a cover slip, imaged at 10x magnification on a compound microscope and counted for the presence or absence of GFP fluorescence in its germline. Numbers represent totals from two separate experiments. The reporter images of live worms were taken of worms treated in a similar manner and visualized on a Leica SP8 scanning laser confocal microscope.

For confocal imaging, germlines were extruded, fixed with 1-2% paraformaldehyde (Electron Microscopy Sciences) and permeabilized with 0.5% Triton-X as previously described (Crittenden et al., 2017). Germlines were incubated with primary antibodies to FLAG (M2® (mouse), Sigma) and GFP (Rabbit anti-GFP, Invitrogen) overnight, stained with fluorophore-labeled secondary antibodies (Alexa 555 Donkey

anti-Mouse, Alexa 488 Goat anti-Rabbit; Invitrogen) and DAPI (Invitrogen), washed and mounted in Vectashield (Vector Laboratories).

For smFISH, gonads were extruded, fixed, and hybridized with single molecule FISH probes as described (Lee et al., 2016). The *gfp* exon probe set contains 38 unique oligonucleotides labeled with CAL Fluor Red 610. Briefly, probes were dissolved in RNase-free TE buffer (10 mM Tris-HCl, 1 mM EDTA, pH 8.0) to create a 250 µM probe stock. Mid-L4 stage animals were grown on OP50 for 24 hours, then dissected in PBS+0.1% Tween-20 + 0.25 mM levamisole. Animals were fixed in 4% paraformaldehyde for 20 minutes, incubated at room temperature in PBS-T (PBS + 0.1% Tween-20) for 10-25 minutes, and equilibrated in smFISH wash buffer (30 mM sodium citrate pH 7.0, 300 mM NaCl, 1% formamide, 0.1% Tween-20, DEPC water) for 10-16 minutes. Samples were then incubated in hybridization buffer (30 mM sodium citrate pH 7.0, 300 mM NaCl, 1% formamide, 10% dextran sulfate w/v, DEPC water) plus 0.5 µM smFISH probe at 37°C for 26-44 hours. 30 nM SNAP 549 ligand was added during the smFISH wash buffer + DAPI wash; samples were washed at 37°C for approximately 60 minutes. Finally, samples were resuspended in 12 µL Antifade Prolong Gold mounting medium (Life Technologies), mounted on glass slides, and cured in a dark drawer for at least 24 hours before imaging.

Samples were imaged using a Leica SP8 scanning laser confocal microscope, taking 0.3 µm (smFISH experiments) or 1 µm (protein staining) slices in sequence. Maximum intensity partial stack projections were generated and brightness adjusted using ImageJ (Schindelin et al., 2015). All images were treated equally in ImageJ and Photoshop, with the exception of the transmitted light images. Imaging experiments were repeated at least twice with similar results, with the exception of PGL-1:SNAP:λN22 K126E K129E worms.

CRISPR-Cas9 guide RNAs and repair oligos

Name	Type	Strain targeted	mutation	Sequence	Enzyme screen
CRISPR-Cas9 guide RNAs:					
glh-1 sgRNA 1	CRISPR-Cas9 sgRNA plasmid	N2	3xmyc	target sequence: TCCACTACCGAATCCAGTTT	
pgl-3 sgRNAin 1	CRISPR-Cas9 sgRNA plasmid	N2	3xV5	target sequence: GCAACGGAACGTCTGGAAG	
pgl-1 crRNA 1	CRISPR-Cas9 RNA	N2	SNAP	target sequence: cccaccagttcagcttatgg	
pgl-1 crRNA 5	CRISPR-Cas9 RNA	JK5687, JK5898, JK5874	K126E K129E	target sequence: gtcttcagtcttcttcagct	
pgl-1 crRNA 8	CRISPR-Cas9 RNA	JK5687	R123E	target sequence: cttcttcagcttggccttac	
SNAP crRNA 1	CRISPR-Cas9 RNA	JK5687	λN22	target sequence: CCTGGGCTGGGTCCTGCAGG	
DNA repair template:					
glh-1 3xmyc repair 1	ssDNA repair oligo	N2	3xmyc	ttccaccggttttattttgattaaaaactttatttcagCgAAAACTGGAAA CGAACAGAAGCTTATTTCCGAGGAAGACCTCGCCG GAGAGCAAAAGCTCATCTCTGAAGAGGATCTTGGAG CCGAACAGAAGCTTATCTCTGAAGAAGACCTCGGAG GATTCGGTAGTGGAGGCGGTTTCGGTGGTGGTAAC AATGGAG	n/a
pgl-3 3xV5 repair 1	ssDNA repair oligo	N2	3xV5	agtttgccagcagcaacggaacCtcCggaCgaggcGGAAAGCCA ATCCCAAACCCACTCCTCGGACTCGACTCCACCGG AGGAAAGCCAATCCCAAACCCACTCCTCGGACTCG ACTCCACCATCGGAAAGCCAATCCCAAACCCACTCC TCGGACTCGACTCCACCGGAtcttatggaggtggtcgcggtgg cgatcgt	BlpI
pgl-1 SNAP	PCR product	JK5687	SNAP	ggattcggtcaatttgctcccaccagttcagcttatggaAGTGGCGGTA TGGACAAAGACTGCGAAATGAAGCGCACCACCCTG GATAGCCCTCTGGGCAAGCTGGAACTGTCTGGGTG CGAACAGGGCCTGCACCGTATCATCTTCCTGGGCAA AGGAACATCTGCCGCCGACGCCGTGGAAGTGCCTG CCCCAGCCGCCGTGCTGGGCGGACCAGAGCCACT GATGCAGGCCACCGCCTGGCTCAACGCCTACTTTC ACCAGCCTGAGGCCATCGAGGAGTTCCCTGTGCCA GCCCTGCACCACCCAGTGTTCCAGCAGGAGAGCTT TACCCGCCAGGTGCTGTGGAAACTGCTGAAAGTGG TGAAGTTCGGAGAGGTCATCAGCTACAGCCACCTG GCCGCCCTGGCCGGCAATCCCGCCGCCACCGCCG CCGTGAAAACCGCCCTGAGCGGAAATCCCGTGCCC ATTCTGATCCCCTGCCACCGGGTGGTGCAGGGCGA CCTGGACGTGGGGGGCTACGAGGGCGGGCTCGCC GTGAAAGAGTGGCTGCTGGCCCACGAGGGCCACA GACTGGGCAAGCCTGGGCTGGGTCCTGCAGGCGG ATCCggaggaggtggtcgcggaggatatggcggtggagaccgtg	n/a
K126E K129E repair	ssDNA repair oligo	JK5687, JK5898, JK5874	K126E K129E	tcgatgacgacaagaagctcggaatgctcgcccgtaaggcTGagctgaa gGagactgaagacgctaagattcttcaagctcttctcaaagt	BlpI
pgl-1 R123E repair	ssDNA repair oligo	JK5687	R123E	tttctgtcatcgatgacgacaagaagctcggaatgctcgcTGAGaaggcc aagctgaagaagactgaagacgctaagattcttc	HpyAV

References

Aoki, S.T., Kershner, A.M., Bingman, C.A., Wickens, M., and Kimble, J. (2016). PGL germ granule assembly protein is a base-specific, single-stranded RNase. Proc Natl Acad Sci USA *113*, 1279-1284.

Arnau, J., Lauritzen, C., Petersen, G.E., and Pedersen, J. (2006). Current strategies for the use of affinity tags and tag removal for the purification of recombinant proteins. Protein Expr Purif *48*, 1-13.

Arribere, J.A., Bell, R.T., Fu, B.X., Artiles, K.L., Hartman, P.S., and Fire, A.Z. (2014). Efficient marker-free recovery of custom genetic modifications with CRISPR/Cas9 in *Caenorhabditis elegans*. Genetics *198*, 837-846.

Brenner, S. (1974). The genetics of *Caenorhabditis elegans*. Genetics *77*, 71-94.

Crittenden, S.L., Seidel, H.S., and Kimble, J. (2017). Analysis of the *C. elegans* germline stem cell pool. Methods Mol Biol *1463*, 1-33.

Gibson, D.G. (2011). Enzymatic assembly of overlapping DNA fragments. Methods Enzymol *498*, 349-361.

Keppler, A., Gendreizig, S., Gronemeyer, T., Pick, H., Vogel, H., and Johnsson, K. (2003). A general method for the covalent labeling of fusion proteins with small molecules *in vivo*. Nat Biotechnol *21*, 86-89.

Lee, C., Sorensen, E.B., Lynch, T.R., and Kimble, J. (2016). *C. elegans* GLP-1/Notch activates transcription in a probability gradient across the germline stem cell pool. Elife *5*, e18370.

Paix, A., Folkmann, A., Rasoloson, D., and Seydoux, G. (2015). High efficiency, homology-directed genome editing in *Caenorhabditis elegans* using CRISPR-Cas9 ribonucleoprotein complexes. Genetics *201*, 47-54.

Schindelin, J., Rueden, C.T., Hiner, M.C., and Eliceiri, K.W. (2015). The ImageJ ecosystem: An open platform for biomedical image analysis. Mol Reprod Dev *82*, 518-529.